

Research project

**A Chandra observation of the  
supernova remnant Cassiopeia A**

Eva Krämer

December 23, 2019

Dr. Karl Remeis–Observatory Bamberg

Astronomical Institute

Friedrich–Alexander–Universität Erlangen–Nürnberg

Supervisor: Prof. Dr. Manami Sasaki

## **Abstract**

A 165 ks observation of the supernova remnant Cassiopeia A performed with the Chandra X-ray observatory was used for a spectral analysis of nine regions. These regions were chosen based on their spectral features seen in different energy bands which were defined around known emission lines from chemical elements. With a simple model for the spectrum chemical abundances for silicon, sulfur, argon, calcium, and iron could be estimated as well as the ionization age and the temperature across the remnant. Chemical abundances appear to be higher than solar, the temperature varies in different regions and the supernova remnant is not in an ionization equilibrium yet.

In addition, the spectrum of the central compact object, a neutron star, was modeled with a simple powerlaw model. The temperature of the surface of the neutron star could be estimated to be  $5.6 \cdot 10^6$  K.

# Contents

<b>1. Introduction</b>	<b>4</b>
<b>2. Astrophysical Background</b>	<b>6</b>
2.1. Supernovae and Supernova remnants . . . . .	6
2.1.1. Supernovae . . . . .	6
2.1.2. Supernova remnant . . . . .	7
2.2. X-rays . . . . .	8
2.2.1. X-ray generating mechanisms . . . . .	8
2.2.2. X-Rays in supernova remnants . . . . .	9
2.2.3. X-rays from Neutron Stars . . . . .	10
2.3. Chandra . . . . .	10
<b>3. Analyzing the spectra of Cas A</b>	<b>12</b>
3.1. Regions . . . . .	12
3.1.1. Model . . . . .	14
3.1.2. Abundances . . . . .	15
3.1.3. Discussion . . . . .	16
3.2. The neutron star . . . . .	18
<b>4. Summary and Outlook</b>	<b>20</b>
<b>A. Appendix</b>	<b>21</b>
A.1. Distribution of elements . . . . .	22
A.2. Three-color images of different energy bands . . . . .	23
A.3. Spectra . . . . .	25

# 1. Introduction

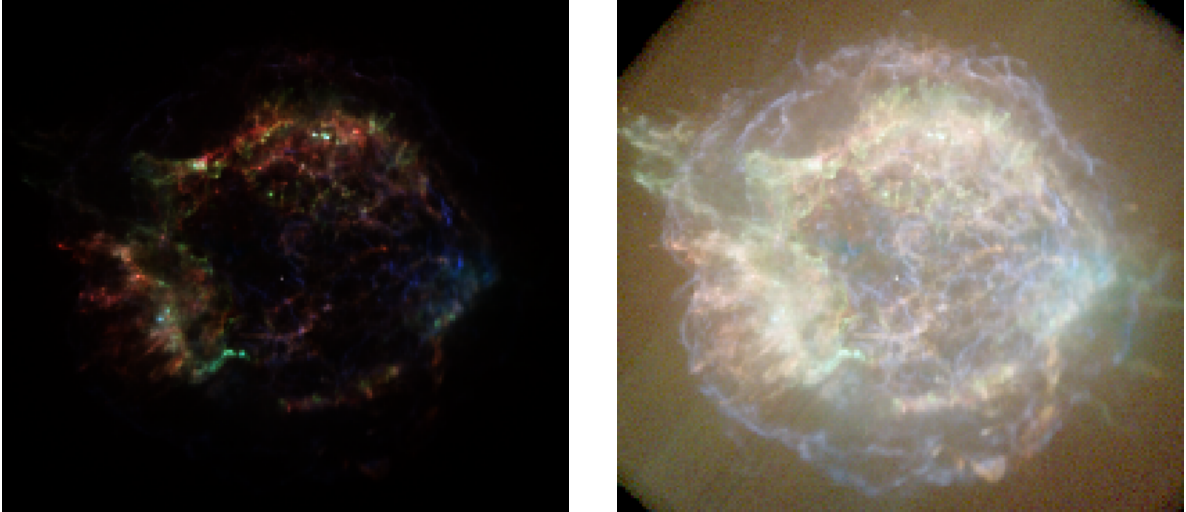


Figure 1.1.: The supernova remnant Cassiopeia A shown in a three-color image. The left panel uses a linear scale for the flux, the right panel a logarithmic scale.

Cassiopeia A is one of the youngest and well studied supernova remnants (SNR). Calculations show that the associated supernova must have taken place around 1680 and it was probably observed by the astronomer John Flemsteed (Reed et al., 1995). Cassiopeia A (in the following referred to as Cas A) has a distance of 3.4 kpc to the Earth and is considered to be the debris of a Type II supernova (Reed et al., 1995). Cas A was discovered as the strongest non thermal radio source apart from the sun (Seward & Charles, 2010). In the X-ray spectrum remarkable features are bright knots and jets outside the debris as seen in Figure 1. A central compact object, a neutron star, was also discovered in Cas A.

X-ray observations of SNR can be used to determine the element abundances in the ejecta and therefore give information about the stellar evolution of the progenitor star and nucleosynthesis during a supernova. The existence of a central compact object gives hints about the type of the supernova and the evolution of the compact object itself.

In the following, the X-ray spectrum of Cas A will be studied and some element abundances determined. There will also be a short section about the neutron star in the center of the remnant.

## 2. Astrophysical Background

In the following chapter an overview of supernova remnants and their evolution as well as the origin of X-rays in such astronomic objects is given. There is also a short introduction to the X-ray spectra of neutron stars and the space telescope Chandra X-ray observatory.

### 2.1. Supernovae and Supernova remnants

In order to understand the observations of a supernova remnant one has to consider their evolution as well as supernovae themselves.

#### 2.1.1. Supernovae

A supernova is the explosion of a star that releases about  $2 \cdot 10^{46}$  J of gravitational energy (Hanslmeier, 2014). One can distinguish between two major types of supernovae: type Ia and core collapse.

There are two scenarios that lead to a type Ia supernova: a white dwarf, that reaches the Chandrasekhar limit or the merger of a binary star, where both components are white dwarfs. Supernovae of type Ia can be observed in all galaxies. There are no hydrogen lines visible in the optical spectrum and the optical light curves reach the same absolute maximum brightness and have a similar shape (Hanslmeier, 2014).

Core collapse supernovae are only observed in spiral galaxies and are the death of a massive star with initial masses  $M > 8 M_{\odot}$ . They burn elements up to iron which has the highest binding energy. After that no exothermic fusion is possible, for that reason the star collapses under its gravity due to the sudden loss of radiation pressure (Hanslmeier, 2014).

### **2.1.2. Supernova remnant**

During a supernova explosion the outer layers of the progenitor star are heated and ejected. These clouds expand into the surrounding interstellar medium and can be seen as bright, extended objects (Seward & Charles, 2010). The evolution of a supernova remnant can be described in three different phases, which will be described in the following paragraphs. A simple model assumes equally distributed ejecta that expand in a uniform interstellar medium (Seward & Charles, 2010).

#### **Free expansion**

In the approximately first 200 years the supernova remnant expands freely into the surrounding interstellar medium. During this phase the fraction of material which is swept up is low compared to the mass of the ejected material (Seward & Charles, 2010).

#### **The adiabatic or Sedov-Taylor phase**

The fraction of swept up material is not negligible anymore, but the radiated energy is still small compared to the internal energy. As the expanding remnant sweeps up material from the interstellar medium a second shock wave, the reverse shock, is formed. It moves inwards and heats the ejected material. Between the outwards moving shock wave and the reverse shock the material is hot (Seward & Charles, 2010).

#### **Radiative phase**

The supernova remnant cools down as it sweeps up more material of the interstellar medium. Most of the internal energy is radiated away and the remnant gets fainter until it can not be distinguished from the surrounding medium anymore (Seward & Charles, 2010).

## 2.2. X-rays

### 2.2.1. X-ray generating mechanisms

There are several mechanisms that can produce X-rays of different types, e.g. thermal radiation, synchrotron radiation, and blackbody radiation. In the following paragraphs, each mechanism is described briefly.

#### Thermal radiation

In a thin, hot ionized gas thermal energy is transferred between ions and electrons through collisions. These cause a change in the trajectory of the colliding particles due to electric forces. The acceleration of the electron leads to electromagnetic radiation in the X-ray regime (Seward & Charles, 2010). This process is called thermal bremsstrahlung and the intensity  $I$  at energy  $E$  and temperature of the gas  $T$  is described by

$$I(E, T) = AG(E, T)Z^2n_in_e\sqrt{kT}e^{-E/kT} \quad (2.1)$$

where  $A$  is a constant,  $n_i$  and  $n_e$  the positive ion number density and electron density,  $Z$  the charge of positive ions,  $k$  the Boltzmann factor and  $G(E, T)$  the Gaunt factor (Seward & Charles, 2010).

In addition, line radiation can be observed if the temperature  $T < 5 \cdot 10^7$  K, because then atoms are not completely ionized (Seward & Charles, 2010). Therefore, a collision can excite an electron in the K or L shell. After the short lifetime of the excited state the ion will relax and, a photon in the X-ray regime will be emitted with a characteristic energy for each element. This can be used to determine element abundances in the supernova remnant.

#### Blackbody radiation

An ideal blackbody is a perfectly absorbing object which also emits radiation only depending on its temperature  $T$ . The intensity of spectrum for a given temperature  $T$  and wavelength  $\lambda$  is given by the Planck's law

$$I(\lambda, T) = \frac{2hc^2}{\lambda^5} \frac{1}{e^{\frac{hc}{\lambda kT}} - 1}, \quad (2.2)$$

where  $h$  is Planck's constant,  $c$  the speed of light and  $k$  the Boltzmann factor (Hanslmeier, 2014).

If the temperature is above  $10^6$  K blackbody radiation in the X-ray regime can be expected (Seward & Charles, 2010).

### **Synchrotron radiation**

Synchrotron radiation is a result of charged relativistic particles moving through a magnetic field. This leads to an acceleration perpendicular to the magnetic field and therefore to the emission of electromagnetic radiation. The energy of the emitted light depends on the velocity of the particle and the strength of the magnetic field (Seward & Charles, 2010).

### **2.2.2. X-Rays in supernova remnants**

Especially in the first two evolutionary phases of a supernova remnant the internal energy is high, which corresponds to a high temperature. Therefore, the elements in the remnant are ionized. The X-ray spectrum of such plasma consists mainly of thermal bremsstrahlung and line radiation (Seward & Charles, 2010).

The plasma of a young supernova remnant is often not in thermal and ionization equilibrium yet, which also has to be considered when modeling the spectrum. Since the plasma is so thin not enough time has passed after the plasma was shocked and only few collisions between particles have occurred. This results in lower ionization states and mimics lower temperatures, since the positive ions have a high temperature while the electrons still have a lower temperature. This can be characterized with the ionization age  $n_e t$ . To reach a collisional ionization equilibrium an ionization age of  $n_e t \approx 10^{12} \text{ s cm}^{-3}$  is needed for supernova remnants (Vink, 2012).

Synchrotron radiation can be expected if there is a strong magnetic field in the remnant. This is for example the case if a pulsar is present (Vink, 2012). Blackbody radiation makes no contribution to the spectrum of a supernova remnant, since the gas is thin and opaque.

### 2.2.3. X-rays from Neutron Stars

If a contracting core of a star reaches the Chandrasekhar limit of  $M \approx 1.4 M_{\odot}$  the pressure of degenerate electrons can not sustain the gravitational force anymore. The stellar core will be compressed even further and a neutron star emerges. They are compact objects with high densities  $\rho \approx 10^{17} \text{ kg m}^{-3}$  and their interior is made of suprafluid neutrons (Hanslmeier, 2014).

Even though a neutron star is not a perfect black body, the shape of the spectrum corresponds to that of a black body, which is modified by the emission of the atmosphere of the neutron star (Seward & Charles, 2010).

A new born neutron star has an initial surface temperature  $T \approx 10^{11} \text{ K}$ , (Seward & Charles, 2010). After 100 years the surrounding supernova remnant expanded sufficiently into the interstellar medium, so the new star can be detected. The neutron star cooled down to a surface temperature  $T \approx 10^6 \text{ K}$ , which corresponds to a peak of a black body spectrum in the X-ray regime (Seward & Charles, 2010).

## 2.3. Chandra

The following section is based on the specifications found on the official website of the Chandra X-ray center (Chandra X-ray Center, 2019).

The Chandra X-ray observatory (in the following referred to as Chandra) is a space telescope which was launched in June 1999. It is especially designed to detect X-ray emission from hot regions of the Universe. Chandra is known for its especially high spatial resolution compared to other X-ray missions such as XMM Newton. Chandra's high Earth orbit is strongly elliptic with a 64 hours orbital period. 85% of Chandra's orbits lies outside the Van Allen radiation belt, therefore uninterrupted observation times up to 55 hours are possible.

Chandra's telescope system consists of four nested mirrors and four scientific instruments: the High Energy Transmission Grating Spectrometer (HETG), the Low Energy Transmission Grating Spectrometer (LETG), a High Resolution Camera (HRC), and the Chandra Advanced CCD Imaging Spectrometer (ACIS). Their assembly is shown in figure 2.3. ACIS and HRC are located at the focal plane of the mirrors. The ACIS is often used for observing extended X-ray sources like supernova remnants.

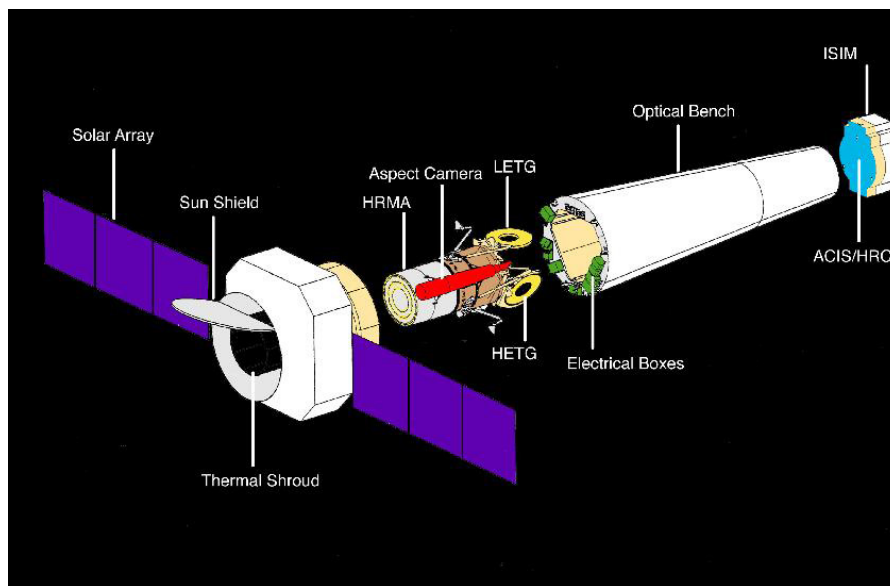


Figure 2.1.: Assembly of Chandra with its mirrors and scientific instruments. Credit: NASA/CXC/SAO

## 3. Analyzing the spectra of Cas A

For the following analysis, data from a 165 ks Chandra observation of Cas A with observation ID 4638 was used. The observation was taken between April 14th and 16th 2004 with the ACIS detector. Data has been obtained from the Chandra X-ray Center. For data reduction and analysis CIAO 4.11 (Fruscione et al., 2006), XSPEC 12.10.1f, and PySPEX 2.0.2 were used.

### 3.1. Regions

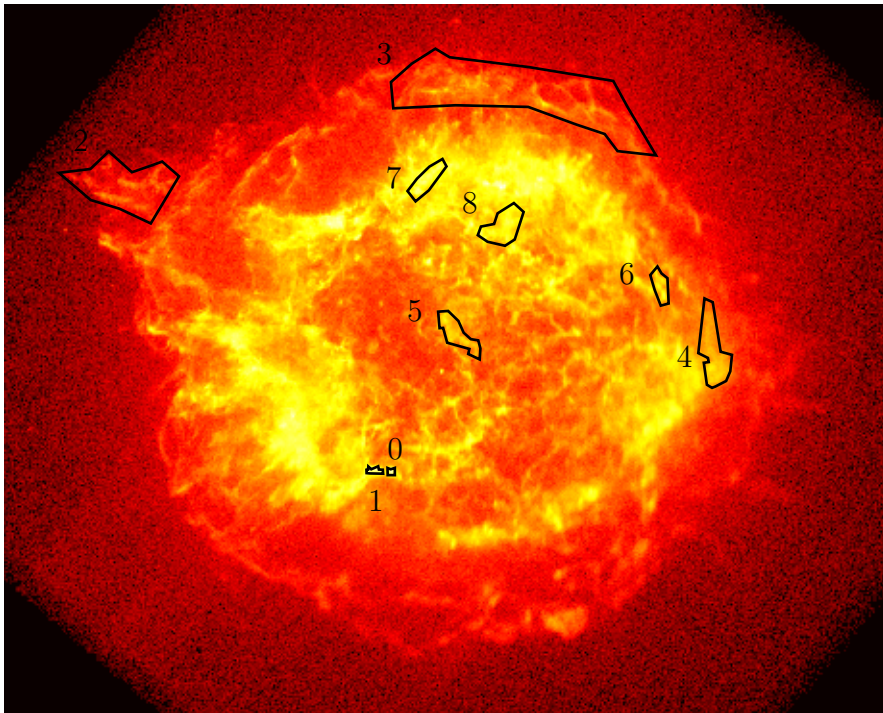


Figure 3.1.: Image of Cas A taken with Chandra ACIS in the energy range of 0.6 – 8.5 keV. Regions used for the spectral analysis are shown in black.

To extract spectra from regions that have especially interesting features, images of the remnant in different energy bands, specified in Table 3.1, were created.

Energy band in keV	associated Element
0.6 – 1.6	Fe L
1.6 – 2.2	Si
2.2 – 2.7	S
2.7 – 3.3	Ar
3.3 – 3.7	<i>Continuum</i>
3.7 – 4.1	Ca
4.1 – 6.2	<i>Continuum</i>
6.2 – 7.0	Fe K
7.0 – 8.5	<i>Continuum</i>

Table 3.1.: The energy bands that were defined to create images, taking the emission lines of different elements into account.

The distribution of the elements can also be seen in images of the remnant in a narrow energy range around known emission lines, shown in Figure A.1. Especially the iron distribution differs from that of the other elements while silicon, sulfur, argon, and calcium are distributed in a similar manner. There are also images of the continuum shown in Figure A.2. In Figure A.3 a difference between the iron K line and iron L line can be seen, indicating that the temperature varies within the supernova remnant. For iron K emission lines higher energies and therefore higher temperatures are required.

We defined nine regions, as shown in Table 3.2 and Figure 3.1, depending on their distinctive features in different energy bands. To get a better notion of regions that show different features in the energy bands, three-color images with different energy bands, shown in Figure A.3, were created. In the following paragraph each region with its distinct features is described.

Region 0 and 1 show strong emission, most likely from lines of silicon and sulfur, but also argon and calcium. Region 2 is part of a jet, a typical feature of Cas A. Region 3 contains only a spectrum of the outer shell and is therefore dominated by the emission caused by the forward shock. Region 4 contains a lot of iron and region 5 is close to the central compact object and should contain unshocked ejecta. Region 6 is especially prominent in the iron K energy band and shows little emission in the iron L energy

band. Region 7 can be associated with a lower temperature and region 8 contains both, hot and cold iron.

Region	special feature
0	knot with a lot of Si,S,Ar,Ca
1	knot with a lot of Si,S,Ar,Ca
2	region in the jet
3	region of the outer shell
4	region with a lot of Fe
5	in the inner part of the shell
6	region with a lot hot Fe
7	region with lower temperature
8	region with both hot and cold Fe

Table 3.2.: The description of the regions that were chosen according to their features

### 3.1.1. Model

The model which was used to fit the spectra consists of two *vpshock* and a *powerlaw* components from XSPEC. To take the absorption of the X-ray photons on their way through space into account, the multiplicative component *TBabs* (Wilms et al., 2000) was used. The *powerlaw* component is a simple photon powerlaw as described in Section 2.2. The *vpshock* component is a plane parallel plasma model with variable abundances (Borkowski et al., 2001). The fit parameters for the first *vpshock* component were set to solar abundances and an initial temperature of  $kT = 1$  keV to model the circumstellar medium. Only the temperature  $kT$ , the ionization age  $\tau_u$ , the redshift and the norm were parameters that were used for the fitting algorithm. The second *vpshock* component was used with variable abundances for silicon, sulfur, argon, calcium, nickel and iron to model the ejecta.

The reduced  $\chi^2$  for the fitting algorithm are shown in Table 3.3 for region 2-6. The remaining regions could not be well fitted with this model. In those cases the fitting algorithm gave reduced  $\chi^2$  of 3 and higher and some parameters could not be fitted well. For those parameters the fitting algorithm gave values at hard limits which could not be avoided even by varying the initial parameters.

In all regions the photon index was used as a parameter for the fitting algorithm with an initial value of 2.7, except for region 2. This initial value was taken from previous models of regions that were only associated with the forward shock. The final results in the regions 3-6 for the photon index did not differ much from that value. In region 2 the photon index of the power law was set to a fixed value of 2.7. This leads to a worse reduced  $\chi^2$  value, but is closer to the values in all the other fitting results and therefore more realistic. In all regions the parameter for magnesium was also used as a fitting parameter, but was then not used except for region 3 because in all other regions it did not show any significant improvement.

Region	Reduced $\chi^2$
2	2.25
3	1.46
4	1.63
5	1.31
6	1.04

Table 3.3.: Reduced  $\chi^2$  values for each fit

### 3.1.2. Abundances

For the regions with reasonable fitting results (region 2-6) an error estimation for the parameters of the second *vpshock* component and the *TBabs* component was made. The results for the 90% error estimation are shown in Table 3.4. The  $kT$  value provides information about the temperature of the plasma in the supernova remnant and  $\tau_u$  is the parameter for the ionization age. The values for the chemical elements are given in solar abundances. The values for the redshift and the norm are also given.

Parameter	Region 2	Region 3	Region 4	Region 5	Region 6
$n_H$	1.3	1.0	2.4	1.5	1.9
[ $10^{22} \text{ cm}^{-2}$ ]	(1.2 – 1.4)	(0.9 – 1.1)	(2.3 – 2.5)	(1.3 – 1.6)	(1.8 – 2.0)
$kT$	2.4	3.9	3.0	2.4	1.2
[keV]	(2.2 – 2.6)	(3.7 – 3.9)	(2.8 – 3.2)	(2.3 – 2.45)	(1.1 – 1.4)
Mg	-	0.56	-	-	-
	-	(0.5 – 0.73)	-	-	-
Si	8.7	1.7	4.4	1.4	1.2
	(8.1 – 9.4)	(1.6 – 1.7)	(4.0 – 4.5)	(1.3 – 1.45)	(1.0 – 1.4)
S	10.6	1.7	5.2	1.2	0.7
	(10 – 11.5)	(1.7 – 1.8)	(4.8 – 5.8)	(1.1 – 1.3)	(0.6 – 1.0)
Ar	10.7	1.5	5.3	1.5	1.4
	(10.0 – 11.5)	(1.2 – 1.7)	(5.0 – 5.6)	(1.3 – 1.6)	(0.5 – 2.4)
Ca	16.7	0.91	6.8	1.3	3.1
	(15.4 – 18.4)	(0.52 – 1.32)	(6.3 – 7.6)	(0.9 – 1.7)	(1 – 5.4)
Fe	2.1	0.65	2.2	0.6	1.2
	(1.8 – 2.4)	(0.60 – 0.74)	(2.1 – 2.3)	(0.5 – 0.7)	(1.0 – 1.7)
$\tau_u$	1.5	0.63	1.9	1.3	11
[ $10^{11} \text{ s cm}^{-3}$ ]	(13 – 15)	(0.60 – 0.74)	(1.8 – 2.0)	(1.2 – 1.5)	(4 – 17)
Redshift	-1.9	-2.7	-2.8	-7.7	-13
[ $10^{-3}$ ]	-(2.0 – 1.7)	-(2.7 – 0.5)	-(3.4 – 2.8)	-(7.9 – 7.5)	-(14 – 11)
Norm	1.7	6.4	7.7	6.5	2.7
[ $10^{-3}$ ]	(1.5 – 1.8)	(6.3 – 6.6)	(6.8 – 8.5)	(6.3 – 6.8)	(2.0 – 3.2)

Table 3.4.: Fit values of the second *vpshock* model component and the *TBabs* component for different regions. Values for chemical elements are given in solar abundances. In brackets the error for the 90 percent confident range is given.

### 3.1.3. Discussion

In the following discussion region 2 will be excluded since the fitting result is not good enough to make assumptions about abundances in this region.

What can be noticed first are the  $\tau_u$  values which represent the ionization age: These values, except in region 6, are below  $10^{12} \text{ s cm}^{-3}$  therefore the supernova remnant is

not in equilibrium yet. The temperature for the second *vshock* component is widely distributed in the range of  $kT = 1.2 - 3.9$  keV, so the temperature varies strongly within the supernova remnant. Region 3 which is associated with the outer shell is the hottest region. While region 6 is the coldest, even though it was expected to be hotter due to strong iron K lines. Region 6 is the region which has the lowest reduced  $\chi^2$  but also with an ionization timescale  $n_e t > 10^{12}$  s cm<sup>-3</sup>. Considering the large 90 % confidence range of  $n_e t$ , this value could have been estimated to high and therefore the actual temperature could be higher, as explained in Section 2.2.2. This would explain the difference between the expected value and the obtained value.

Region 3, which is associated with the forward shock only, shows higher abundances for silicon, sulfur, and argon but lower values for iron and magnesium. In region 4 all elements are enriched, especially iron. This region has the highest iron abundance of all considered regions, as expected from the three-color images in Figure A.3. Region 5 which belongs to the yet unshocked ejecta shows little iron but all other abundances are slightly higher. Region 6 especially shows strongly enriched calcium as expected from the images of the energy bands in Figure A.1. Overall the iron distribution varies strongly across the remnant and the element abundances for silicon, sulfur, argon and calcium are higher than those in the sun.

This model could not describe the regions which were associated with strongly enriched silicon, sulfur, argon, and calcium. If a different model is chosen for those region one might be able to make assumptions about abundances in these regions and thus for the ejecta. Since jets are not part of the standard model for the evolution of supernova remnants, another model might be better suited to describe the physics which lead to such phenomena.

Since this model only gave a good result for the fit in one case, namely region 6, all assumptions made above should be investigated further with more regions or a better suited model.

## 3.2. The neutron star

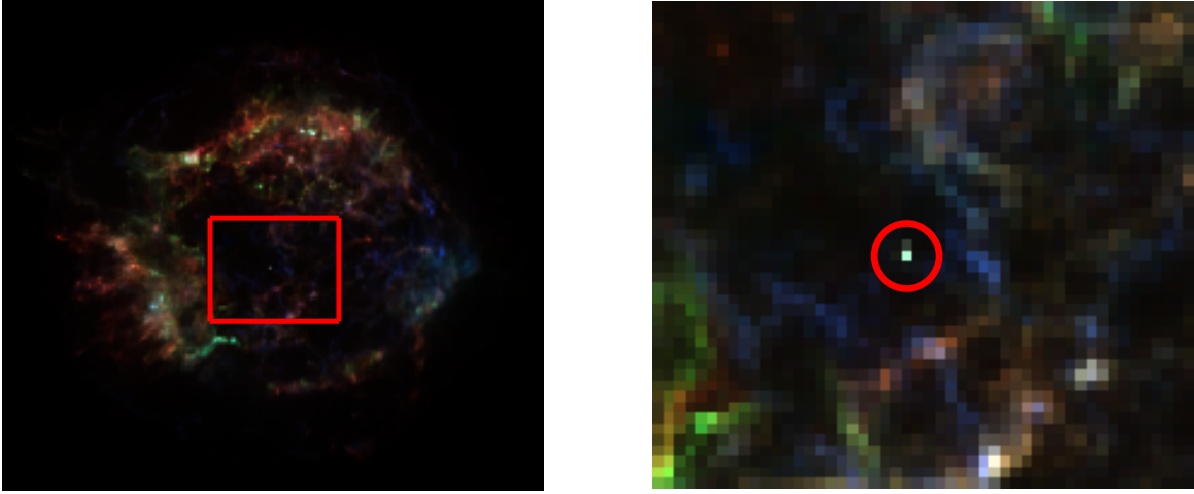


Figure 3.2.: The center of the SNR. One bright pixel can be seen which is considered to be a neutron star.

In the middle of the SNR Cas A a point-like source has been detected (Tananbaum, 1999), as can be seen in Figure 3.2. Even though the remnant has been observed with many other telescopes only with Chandra the central compact body could be resolved and identified as a neutron star due to the better spatial resolution (Ho & Heinke, 2009). The spectrum of the neutron star, shown in Figure 3.3, can be modeled with a blackbody emission spectrum as described in Section 2.2.1. When fitting this model with the multiplicative component *TBabs* (Wilms et al., 2000), the spectrum is best described with the parameters given in Table 3.2. The fitting algorithm gives a reduced  $\chi^2 = 1.48$ .

Parameter	Value	90 % confident range
$kT$ in keV	0.48	0.47 – 0.49
Norm in $10^{-5}$	2.4	2.2 – 2.4

Table 3.5.: Fit values and their 90 % confident range for the neutron star spectrum. The model *TBabs\*body* in XPEC was used.

The  $kT$  value of the fitted model in Table 3.2 corresponds to a Temperature of

$$T = 5.6 \cdot 10^6 \text{ K.}$$

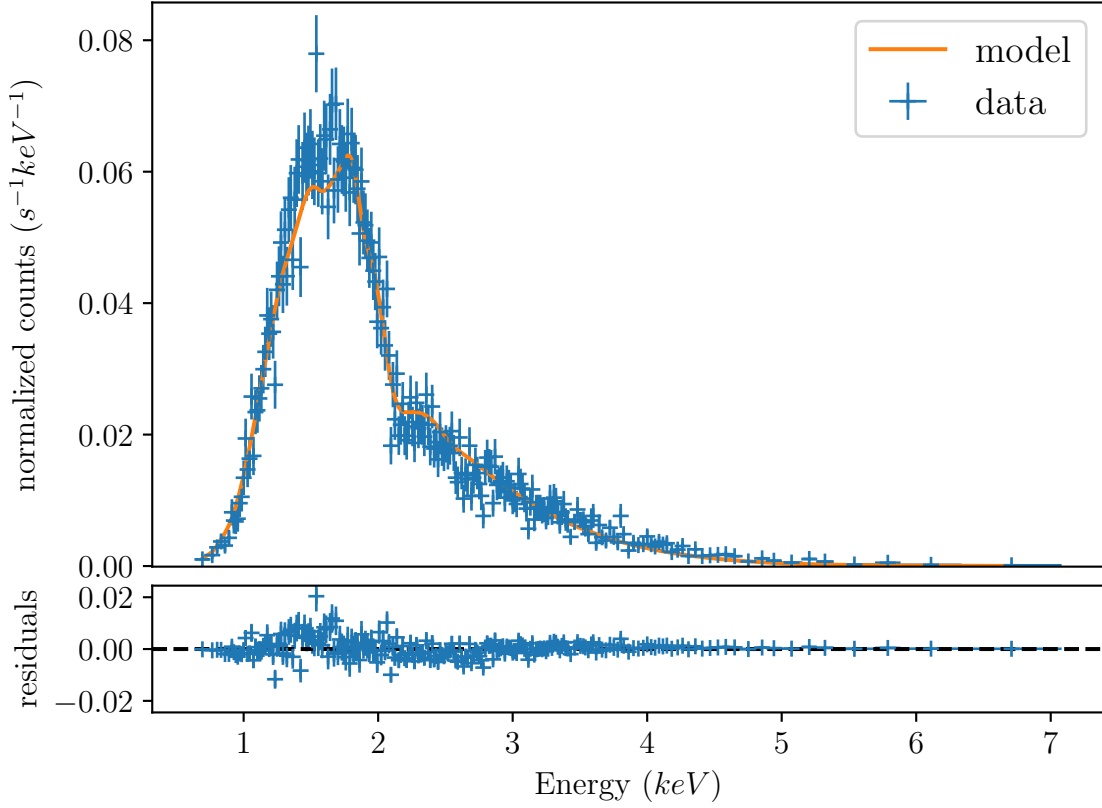


Figure 3.3.: The spectrum of the neutron star. Modeled with  $TBabs*bbbody$  from XSPEC. The fit has a reduced  $\chi^2$  of 1.48.

This temperature is 2.7 times higher than the one calculated by C. Heinke and H. Wynn in 2009. For their non-magnetic carbon atmosphere model they calculated a temperature of  $2.04 \cdot 10^6$  K (Heinke & Ho, 2010). This difference can be explained by the different models that were used. Using only a blackbody model is a simplification, that does not take into account the stellar atmosphere or effects due to magnetic fields. This also explains the rather high reduced  $\chi^2$ , which indicates that the spectrum might be described better with a different model.

## 4. Summary and Outlook

Cassiopeia A is a supernova remnant that shows a lot of different features. The remnant is strongly asymmetric and only few regions correspond well to the chosen spectral model. The remnant is not in ionization equilibrium yet, overall chemical abundances are higher than solar abundances and the iron distribution varies across the remnant. To get a better notion of these abundances one should consider looking at more regions that are close to the selected ones or show similar features.

In order to get a better understanding of the spectrum of Cas A one should also consider using a different model. It might be useful to apply models depending on the location of the region: forward shock only, ejecta or part of the jet.

The neutron star can be modeled with a blackbody spectrum. Choosing a more detailed model which takes other effects into account would help to get better results.



# A. Appendix

## A.1. Distribution of elements

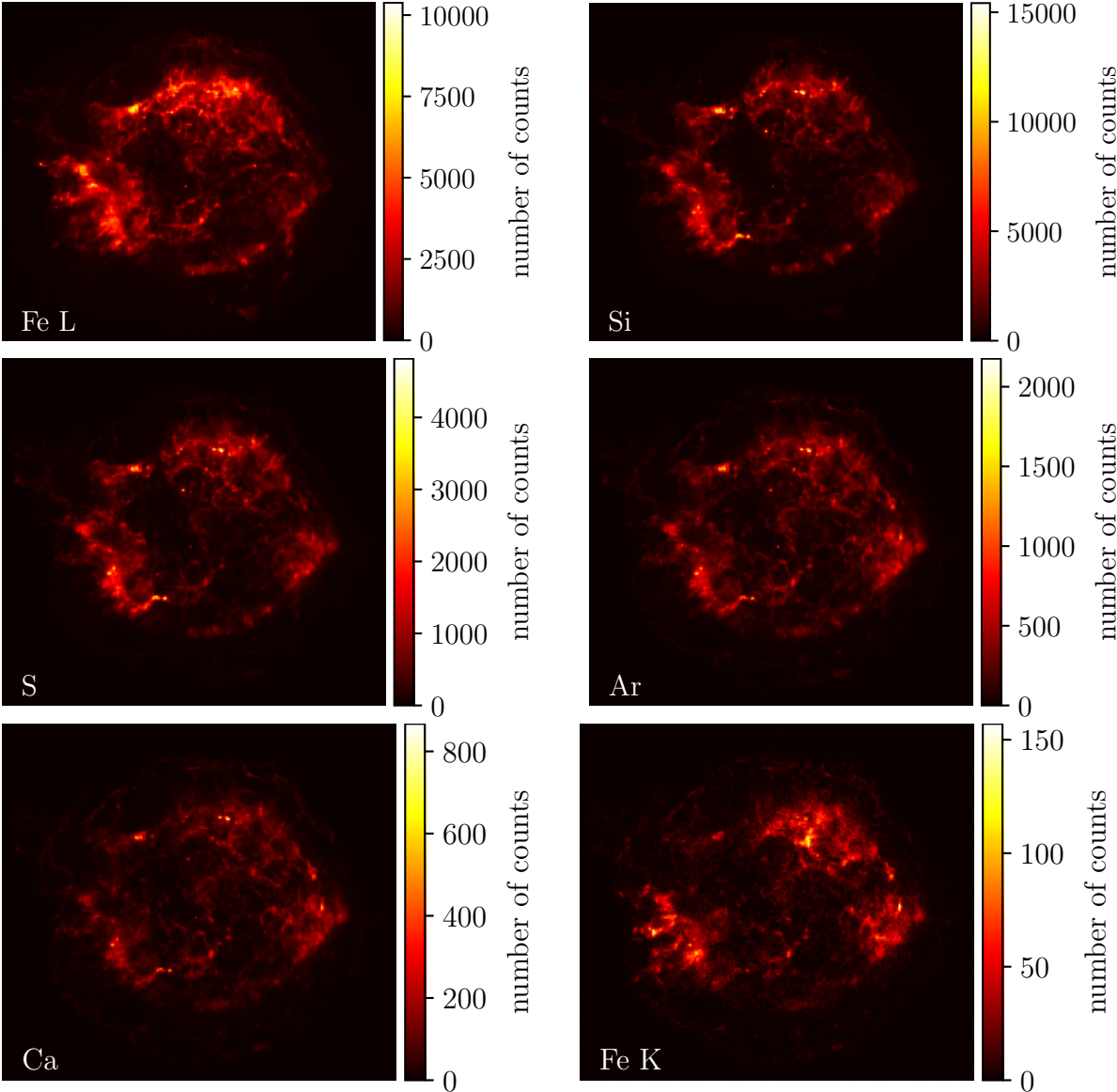


Figure A.1.: Cassiopeia A in different energy bands that include the emission lines of iron, silicon, sulfur, argon, and calcium.

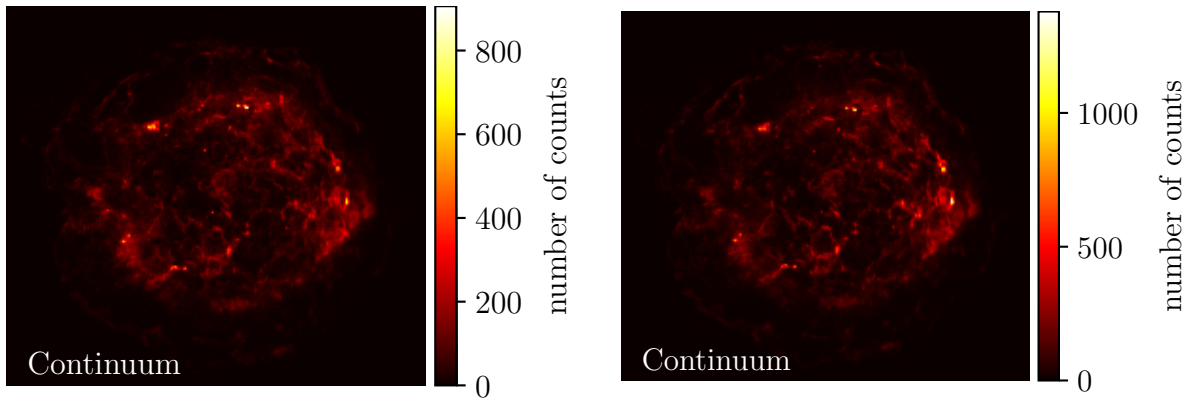


Figure A.2.: Continuum images of Cas A (left: 3.3 – 3.7 keV, right: 4.1 – 6.2 keV).

## A.2. Three-color images of different energy bands

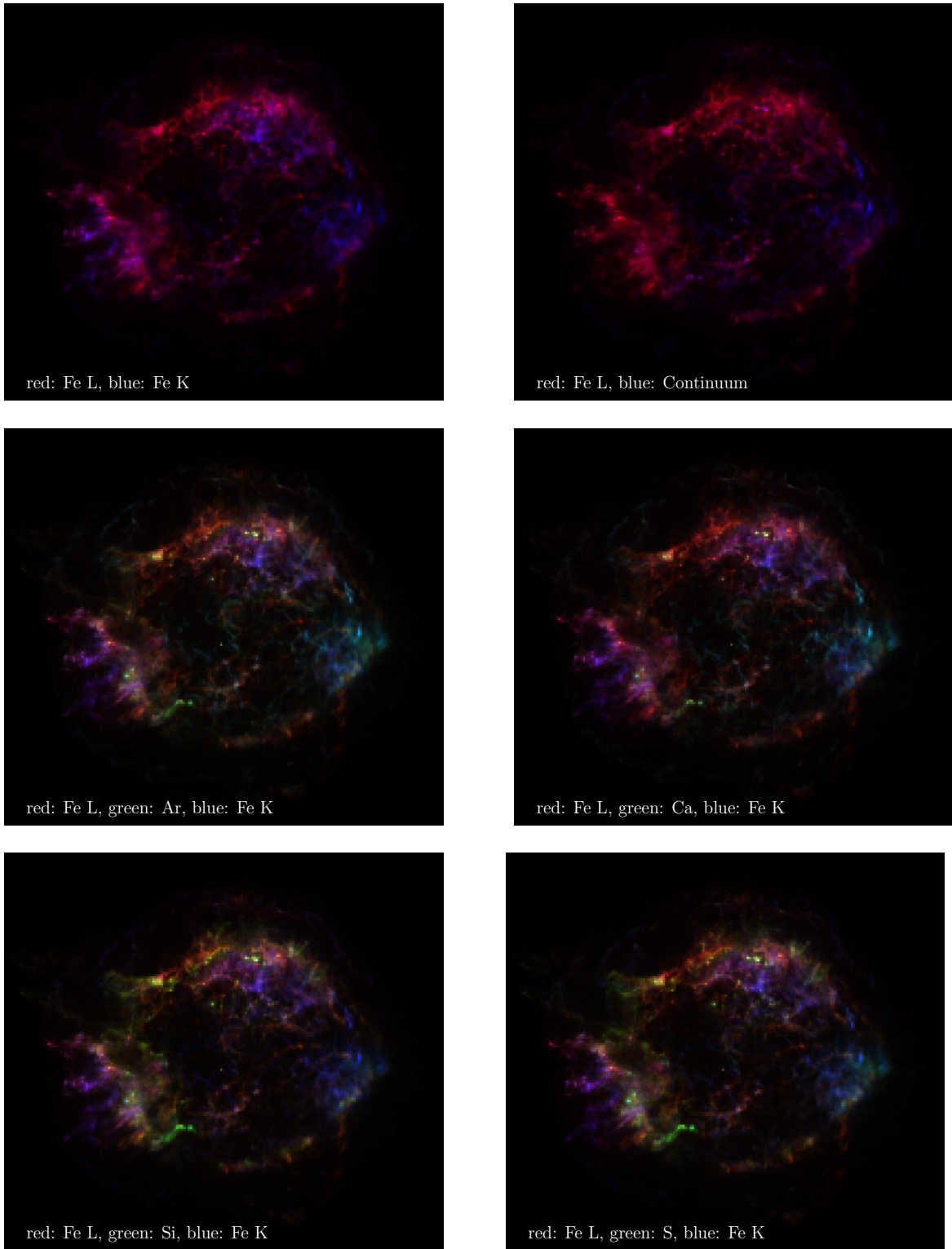


Figure A.3.: Three-color images of Cas A in different energy bands to highlight the differences in the element distribution.

### A.3. Spectra

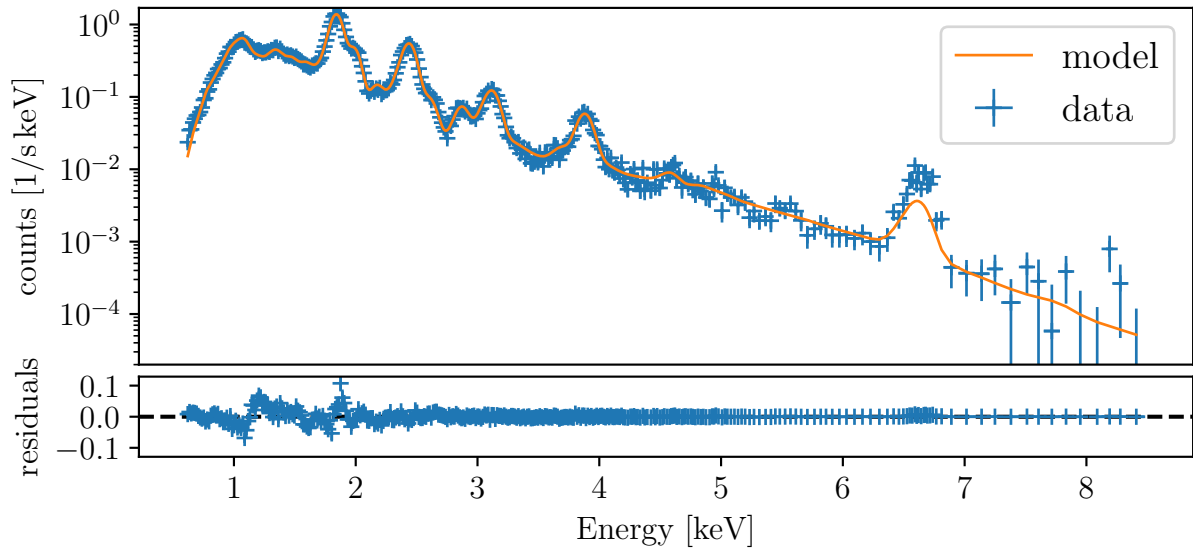


Figure A.4.: Spectrum of Region 2 with a reduced  $\chi^2 = 2.25$ . This region is part of the jet.

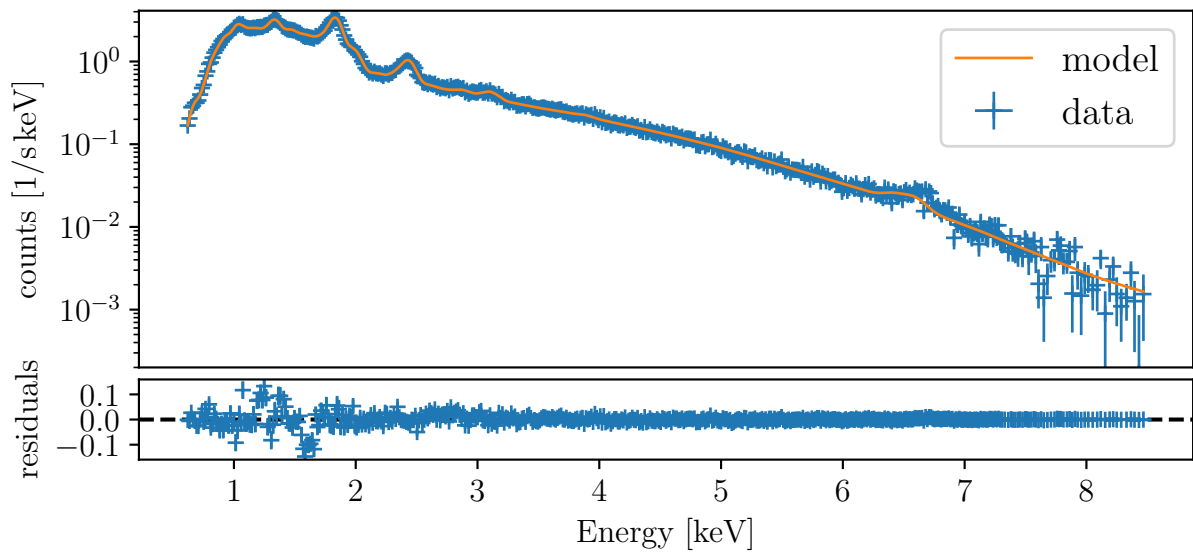


Figure A.5.: Spectrum of Region 3 with a reduced  $\chi^2 = 1.46$ . This region is part of the outer shell and is therefore associated with the forward shock.

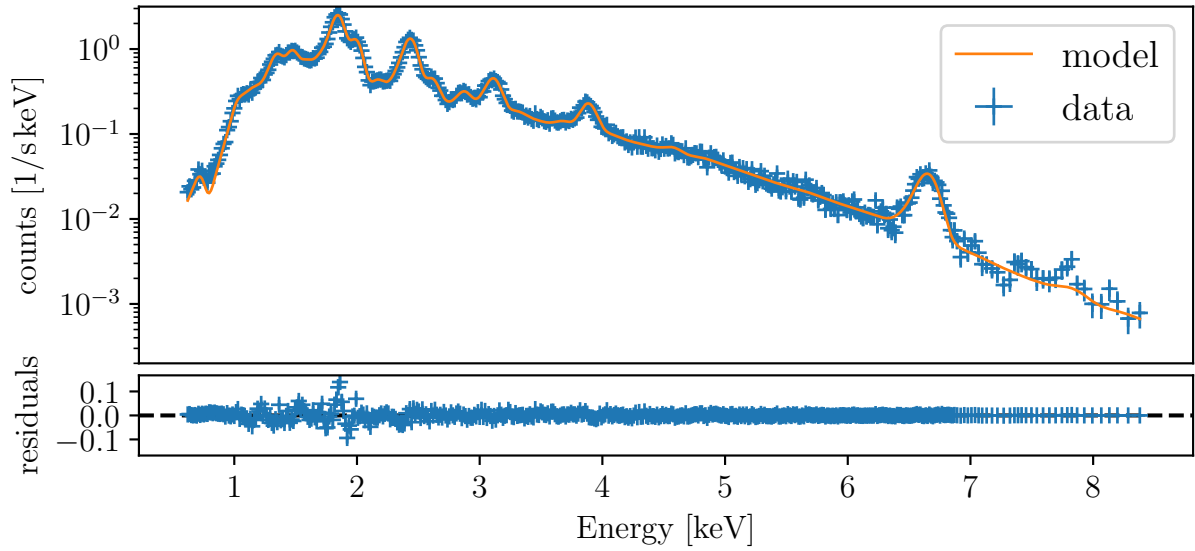


Figure A.6.: Spectrum of Region 4 with a reduced  $\chi^2 = 1.63$ . In this region a lot of iron is expected.

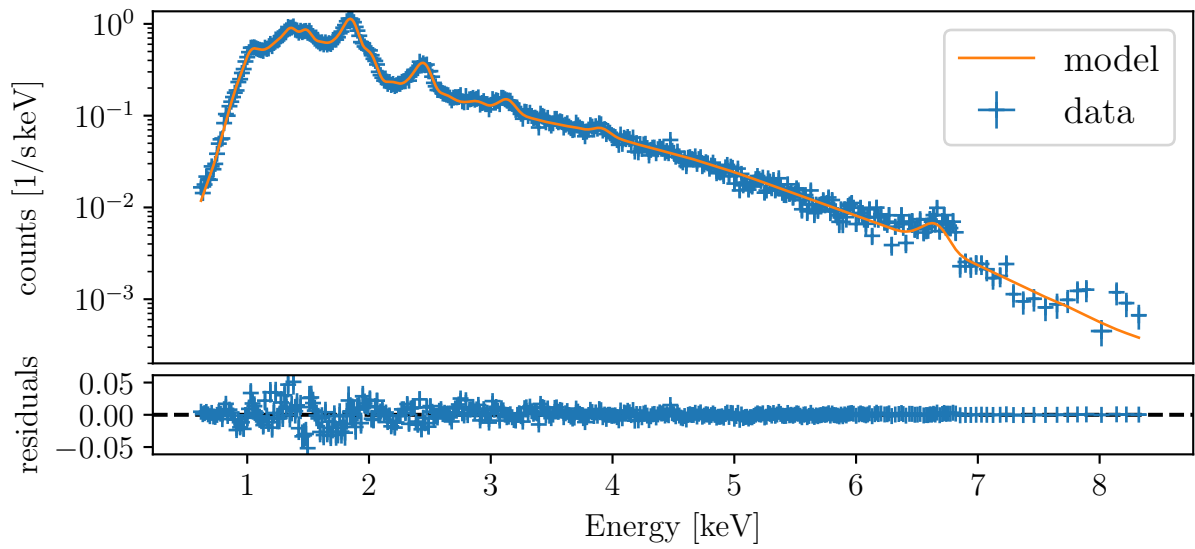


Figure A.7.: Spectrum of Region 5 which lies in the inner part of the shell near the neutron star with a reduced  $\chi^2 = 1.31$ .

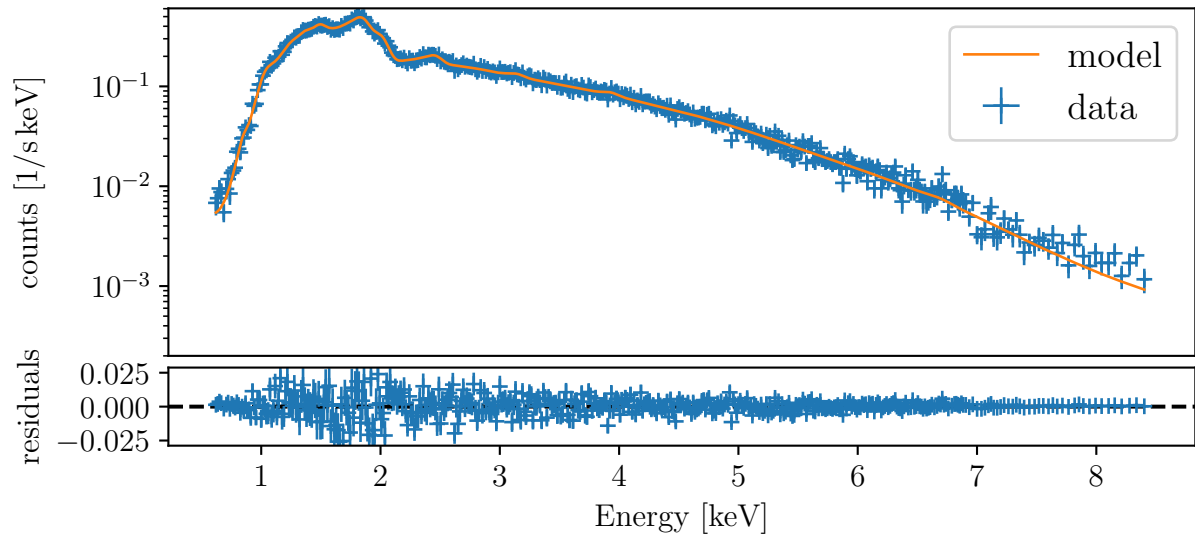


Figure A.8.: Spectrum of Region 6 with a reduced  $\chi^2 = 1.04$ . In this region a lot of hot iron is expected.

# Bibliography

- Borkowski, K. J., Lyerly, W. J., & Reynolds, S. P. 2001, *The Astrophysical Journal*, 548, 820, doi: 10.1086/319011
- Chandra X-ray Center. 2019, Chandra X-Ray observatory - About chandra. <https://chandra.harvard.edu/about/>
- Fruscione, A., McDowell, J. C., Allen, G. E., et al. 2006, *Society of Photo-Optical Instrumentation Engineers (SPIE) Conference Series*, Vol. 6270, CIAO: Chandra's data analysis system, 62701V
- Hanslmeier, A. 2014, *Einführung in Astronomie und Astrophysik*
- Heinke, C. O., & Ho, W. C. G. 2010, *The Astrophysical Journal*, 719, L167, doi: 10.1088/2041-8205/719/2/1167
- Ho, W. C. G., & Heinke, C. O. 2009, *Nature*, 462, 71
- Reed, J. E., Hester, J. J., Fabian, A. C., & Winkler, P. F. 1995, *The Astrophysical Journal*, 440, 706, doi: 10.1086/175308
- Seward, F. D., & Charles, P. A. 2010, *Exploring the X-ray Universe*, 2nd edn. (Cambridge University Press), doi: 10.1017/CB09780511781513
- Tananbaum, H. 1999, *International Astronomical Union Circular*, 7246
- Vink, J. 2012, *Astronomy and Astrophysics Reviews*, 20, 49, doi: 10.1007/s00159-011-0049-1
- Wilms, J., Allen, A., & McCray, R. 2000, *The Astrophysical Journal*, 542, 914, doi: 10.1086/317016